Supporting Information

Cheng et al. 10.1073/pnas.1612106114

SI Models and Methods

Here, we simulate the water/Cu(100) interface using 48 explicit water molecules (five layers, 1.21 nm thick) on a 4 × 4 Cu(100) surface slab (three layers) with an area of 1.02 nm^2. To equilibrate the waters interacting with the interface, we carried out 2 ns of reactive molecular dynamics (RMD) simulations using the ReaxFF reactive force field for Cu and H_2O (39). Starting from this well-equilibrated interface, we carried out 10 ps of ab initio AIMD simulation at 298 K. After that, we used metadynamics and thermodynamic integration to calculate free-energy barriers for various reaction steps (the results were averaged over three independent calculations). We find that including one extra Na solvated in the solution leads to a work function of 3.40 (±0.25) eV, which corresponds to −0.59 V (RHE) (3.40 − 4.40 + 0.0592 × 7 = −0.59 V), close to the potential [−0.60 V (RHE)] with maximum C_2H_4 production at pH 7 (11). The simulation box is 40 Å along the z axis with a vacuum of 24 Å. The lateral dimensions of the slab were fixed using the 3.61-Å lattice constant. Two CO molecules and one H atom were placed on the 4 × 4 unit cell (on top site) corresponding to a surface coverage of 1/8 and 1/16 ML, respectively. A snapshot of the simulation box is shown in Fig. S1. We consider that this model of QM with explicit treatment of the water dynamics at operating temperature provides a representative description of the reaction kinetics.

We considered both the Eley–Rideal (ER) and Langmuir–Hinshelwood (LH) reaction mechanisms. In ER, $H_2O + e^-$ are used in the reduction reaction (e^- is used implicitly). In LH, surface hydrogen (H*) is used in the reduction reaction. For LH, the formation of H* implicitly involves either H_3O^+ or OH^-, so that both the reaction barrier ($\Delta G^{\ddagger}$) and the energy (ΔG) are pH dependent. At pH 7, the $\Delta G^{\ddagger}$ and ΔG of reactions via LH are corrected by 0.41 eV (0.0592 × 7) to compare with the ER reactions.

Electronic structure calculations were performed within the DFT framework, as implemented in the Vienna ab initio simulation program (VASP) (42–45), a plane-wave pseudopotential package. The exchange and correlation energies were calculated using the Perdew, Burke, and Ernzerhof (PBE) functional within the generalized gradient approximation (GGA) (46, 47). Spin polarization did not have an appreciable effect on the overall energies. For example, the total energies are different by less than 0.01 eV for adsorbed hydrogen (H*) on Cu(100) surface. The calculations were therefore carried out without spin polarization to reduce computational demands.

We used a plane-wave cutoff energy of 400 eV and the first-order Methfessel–Paxton scheme with a smearing width of 0.2 eV. Dipole corrections were applied along the z axis. The PBE-D3 method was used to correct van der Waals interaction of water–water and water–Cu (48). The energy minimization criterion was that all forces on free atoms be <0.02 eV/Å. The charges on various species were derived using a Bader analysis (49).

We used a 1.2-fs time step in the molecular dynamics (MD) simulations with the hydrogen mass set to 2 atomic mass units. These MD simulations used only the gamma point of the Brillouin zone with no consideration of symmetry. The velocities were rescaled every 20 MD steps to readjust the target temperature to equilibrium. We used a Nose–Hoover thermostat for the free-energy calculations with a temperature damping parameter of 100 fs.

Enhanced sampling methods can increase the timescale of brute force simulations. We calculated the free energies using metadynamics (14, 15) and constrained molecular dynamics (16) (blue moon ensemble). Three parameters are controllable and relevant to the accuracy of a metadynamics simulation: height of a Gaussian hill (h), the width of the Gaussian hill (ω), and frequency to update the bias potential (t_G) (40, 41). We used an ideal double-well model with a transition barrier of 0.9 eV to derive the optimal parameters for the best balance of accuracy and efficiency. In this work, these parameters are h = 0.08 eV, ω = 0.18 Å, and t_G = 24 fs. For the constrained molecular dynamics, we used an increment of 0.67×10^{-3} Å/fs to the collective variables. We found that simulation times of 2.4–9.6 ps were sufficient to complete the reaction, depending on the reaction pathways.

From the reactive trajectories, we selected 11 windows for thermodynamic integration calculations. The 2.4-ps simulations were carried out at each window to produce the potential of mean force (PMF). Energy profiles were obtained by integrating the PMF. More simulation details and definitions of collective variables (CVs) for elementary reactions are in *SI CVs and Free-Energy Barriers*. In this work, we calculate the Helmholtz free energies (F), which we assume are similar to the Gibbs free energies (G).

The strategies used to enhance ensemble averaging were as follows: (*i*) We carry out 2 ns of reactive molecular dynamics (RMD) simulations using the ReaxFF reactive force field to equilibrate the water/Cu(100) interface. This ReaxFF simulation is necessary because the relaxation time of water at the interface is much longer than in bulk. (*ii*) We carry out three independent simulations to reduce any bias that might arise from specific water configurations. (*iii*) We use thermodynamic integration (TI) as an efficient way to extend the short metadynamics simulations. These TI calculations convert the serial calculation into windows that can be calculated in parallel.

In all of the cases (except C–C coupling), the difference between the current step and next step is only one hydrogen, which we consider as a too small perturbation to induce large surface reorientations. The most significant change we observe in the water structure at the surface is the readjustment of hydrogen bond network, which is captured within 2 ps in our explicit water description, which facilitates proton transfer to the stable position by formation hydrogen bond network (an advantage of simulations with explicit H_2O). At each step, one additional hydrogen was added either on the surface (if H* was consumed) or in bulk (if H_2O provides the proton). In the case of adding H*, the closest available hollow (fourfold) site was chosen to deposit the H*. A 2-ps AIMD simulation was then carried out to equilibrate the system. In the case of adding a proton to bulk solvent, one H was added to one surface H_2O (vacuum/H_2O interface) to form H_3O^+, which was neutralized during the AIMD by the OH^- produced through the hydrogen-bond network in a 2-ps AIMD equilibration. The configuration produced provides a reasonable representation of the reactant for the next reduction step.

For steps where the surface H (H*) model was used to locate transition states, we referenced the initial states back to the $H^+(H_3O^+/H_2O) + e^-$ pair through free-energy differences between H* and H_2(g), based on the half-cell reactions ($H^+ + e^- \rightarrow$ H*). Thus, the pH effect is introduced by applying a correction of 0.41 eV (7 × 0.0592) to free-energy barriers and free-energy differences.

For reactions where H_2O acts as the proton source with the release of OH^-, the pH enters the free-energy profiles naturally as the reactant or product (no correction).

To compare with the constant potential of experiments, we used the procedure proposed by Chan and Nørskov (50) to

remove any artifacts involving work function changes during the chemical reaction. Because we considered the charges in plane-wave calculations to be suspect, we replaced the charge with the calculated capacitance (more details in *SI Constant Potential Corrections*). For the cases reported here, these corrections of the free-energy barriers were insignificant (<0.02 eV).

SI Metadynamics

The metadynamics Hamiltonian $\tilde{H}(p,q,t)$ is written as follows:

$$\tilde{H}(p,q,t) = H(p,q) + \tilde{V}(t,\xi), \quad \text{[S1]}$$

where p, q, and t is generalized momenta, generalized coordinate, and time. $H(p,q)$ is the Hamiltonian for the original (unbiased) system, ξ is the CV, and $\tilde{V}(t,\xi)$ is the time-dependent bias potential. The bias term is defined as a sum of deposited Gaussian functions as follows:

$$\tilde{V}(t,\xi) = h\sum_{i=1}^{t/t_G} \exp\left\{-\frac{\left|\xi^t - \xi^{(i\cdot t_G)}\right|^2}{2\varpi^2}\right\}. \quad \text{[S2]}$$

Here, h and ω are the height and width of the Gaussian function. t_G is the time interval to add a new Gaussian. The summation represents the history-dependent potential acting on the current values of the ξ. The biased potential is related to the free energy via the following:

$$A(\xi) = \lim_{t\to\infty} \tilde{V}(t,\xi) + \text{const.} \quad \text{[S3]}$$

In principle, smaller perturbations would lead to better accuracy, but this would require longer simulation times. Although many papers have been published discussing how to choose the parameters (23, 24), there is still no general rule. One must consider each specified case. In this work, we used an ideal double-well model with a transition barrier of 0.9 eV to derive the optimal parameters for the best balance of accuracy and efficiency, as shown in the following: h = 0.08 eV; ω = 0.18 Å; and t_G = 20 time steps.

We carried out metadynamics simulations until the first barrier crossing.

SI Constrained Molecular Dynamics (25)

The correct (unbiased) average for a quantity $\alpha(\xi)$ of constrained (biased) molecular dynamics can be obtained as follows:

$$\alpha(\xi) = \frac{\left\langle \sqrt{Z}\cdot\alpha(\xi^*)\right\rangle_{\xi^*}}{\left\langle\sqrt{Z}\right\rangle_{\xi^*}}, \quad \text{[S4]}$$

where Z is a mass metric tensor defined as follows:

$$Z_{\alpha,\beta} = \sum_{i=1}^{3N} m_i^{-1}\nabla_i\xi_\alpha\cdot\nabla_i\xi_\beta,\ \alpha = 1,\ldots,N,\ \beta = 1,\ldots,N, \quad \text{[S5]}$$

and the free-energy gradient can be computed using the following equation (25):

$$\left(\frac{\partial A}{\partial\xi_k}\right)_{\xi^*} = \frac{1}{\left\langle\sqrt{|Z|}\right\rangle_{\xi^*}}\left\langle\sqrt{|Z|}\left[\lambda_k + \frac{k_B T}{2|Z|}\sum_{j=1}^{r}\left(\frac{1}{Z}\right)_{kj}\times\sum_{i=1}^{3N}\frac{\nabla_i\xi_j\cdot\nabla|Z|}{m_i}\right]\right\rangle_{\xi^*}, \quad \text{[S6]}$$

The free-energy difference between states 1 and 2 can be calculated by integrating the free-energy gradients over a connecting path:

$$\Delta A_{1\to2} = \int_{\xi(1)}^{\xi(2)}\left(\frac{\partial A}{\partial\xi}\right)_{\xi^*} d\xi. \quad \text{[S7]}$$

We first used slow growth to generate the reaction path. We applied an increment of 0.0008 Å/step (or 0.00067 Å/fs) to CVs to drive the chemical reactions. We found that simulation times of 2.4–9.6 ps were necessary to complete the reaction, depending on the length of reaction pathways. From the reactive trajectories, we selected 11 windows for thermodynamic integration calculations. Simulations of 2.4 ps were carried out at each window to produce the PMF. Energy profiles were obtained by integrating the PMF.

SI CVs and Free-Energy Barriers

In free-energy calculations, the CVs are the distance between hydrogen (H) and carbon (C) [R(C–H)], the distance between H and oxygen (O) [R(O–H)], or the distance between C and O [R(C–O)]. The distances are a natural choice for the LH model. The ER model is more complex than LH model because the proton transfer procedure involves a hydrogen-bond (HB) channel established by several water molecules. In our previous work with H_3O^+ (pH 0), we used a CV defined by HB bond network. In this work, the simulation is at pH 7. Therefore, the proton is provided by an H_2O. For example: at pH 7, the Volmer reaction is $H_2O + e^- \rightarrow H^* + OH^-$. In this condition, we found R(O–H) or R(C–H) [C (or O) is from intermediates and H is from the nearest water] is sufficient for defining a CV, because the subsequent proton transfer reactions can occur in brute-force simulation due to the low energy barriers of proton transfer (about 0.15 eV based on our previous calculation) (12).

The CV and $\Delta G^{\ddagger}$ of elementary reaction in CH_4 formation and C_2H_4 formation are shown in Tables S1 and S2.

SI Constant Potential Corrections

The simulations are done at constant charge [the number of electrons (N_e) is fixed], which means that the work functions (Φ) change along the reaction pathway. For a simulation starting with Φ_1 and ending with Φ_2, the electrostatic energy change ($\Delta E^{electrostatic}_{\Phi_2-\Phi_1}$) can be determined by the modification of the charges ($\Delta q = q_2 - q_1$) and the change in the work functions ($\Delta\Phi = \Phi_2 - \Phi_1$) by using the correction method proposed by Chan and Nørskov (50):

$$\Delta E^{\text{electrostatic}}_{\Phi_2-\Phi_1} = \frac{(q_2-q_1)(\Phi_2-\Phi_1)}{2} = \frac{\Delta q\cdot\Delta\Phi}{2}. \quad \text{[S8]}$$

However, for plane-wave calculations, the atomic charges are ambiguous. Instead, we use the capacitance (C) to replace change (q), which can be calculated from the work function change as the total number of electrons is varied:

$$C = \frac{\Delta q}{\Delta\Phi}. \quad \text{[S9]}$$

We calculate C from the shift in the work function as the number of total electrons is varied. For the Cu(100) bare surface, the calculated C is 0.79 e/V. The reaction intermediates have a slight influence on C ranging from 0.79 e/V to 0.83 e/V. Therefore, we use one C value (0.79 e/V) in our calculation. Φ is related to the absolute potential (U) vs. the standard hydrogen electrode via the following:

$$U = \frac{\Phi - \Phi_{SHE}}{e}. \quad \textbf{[S10]}$$

Therefore,

$$\Delta\Phi = \Delta U \cdot e. \quad \textbf{[S11]}$$

Inserting Eqs. **S9** and **S11** into Eq. **S8** leads to the following:

$$\Delta E^{electrostatic}_{U_2-U_1} = \frac{C \cdot e^2 \cdot \Delta\Phi^2}{2}. \quad \textbf{[S12]}$$

SI Formation of Acetate

The noticeable amounts acetate (CH_3COO^-) formation was observed in the work of Li et al. (37) using oxide-derived Cu nanoparticle as catalysts for CO reduction. In their work, the authors proposed that the formation of acetate probably arises from an attack of OH^- on a surface-bound ketene or another carbonyl-containing intermediate after C–C bond formation. Instead, we propose that the acetate formation may involve surface O* attacking surface-bond α-hydroxy ketone (*COH–C=O) as follows:

$$*COH\text{–}C=O + O^* + e^- \xrightarrow[1.07]{} *COH\text{–}COO^-, \quad \textbf{[S13]}$$

$$*COH\text{–}COO^- + e^- \xrightarrow[0.91]{} *C\text{–}COO^- + OH^-, \quad \textbf{[S14]}$$

$$*C\text{–}COO^- + H^* \xrightarrow[1.01]{} *CH\text{–}COO^-, \quad \textbf{[S15]}$$

$$*CH\text{–}COO^- + H^* \xrightarrow[1.29]{} *CH_2\text{–}COO^-, \quad \textbf{[S16]}$$

$$*CH_2\text{–}COO^- + H^* \xrightarrow[1.59]{} CH_3COO^-(aq). \quad \textbf{[S17]}$$

SI Probe Molecules

Ethylene oxide (C_2H_4O) and glyoxal ($C_2H_2O_2$) were used experimentally as probe molecules to supply auxiliary information about the mechanism of ethylene formation. The following are the lowest kinetic pathways for the ethylene formation from ethylene oxide and acetaldehyde or ethanol formation from glyoxal predicted from free-energy calculations.

Ethylene Oxide.

$$C_2H_4O(aq) + H_2O + e^- \xrightarrow[0.48]{} *CH_2\text{–}CH_2OH + OH^-, \quad \textbf{[S18]}$$

$$*CH_2\text{–}CH_2OH + e^- \xrightarrow[0.17]{} *CH_2=CH_2 + OH^-. \quad \textbf{[S19]}$$

Glyoxal.

$$CHO\text{–}CHO(aq) + H_2O + e^- \xrightarrow[0.75]{} *CHOH\text{–}CHO + OH^-, \quad \textbf{[S20]}$$

$$*CHOH\text{–}CHO + H^* \xrightarrow[1.21]{} *CH_2OH\text{–}CHO, \quad \textbf{[S21]}$$

$$*CH_2OH\text{–}CHO + e^- \xrightarrow[0.43]{} *CH_2\text{–}CHO + OH^-, \quad \textbf{[S22]}$$

$$*CH_2\text{–}CHO + H_2O + e^- \xrightarrow[0.58]{} CH_2=CHOH + OH^-. \quad \textbf{[S23]}$$

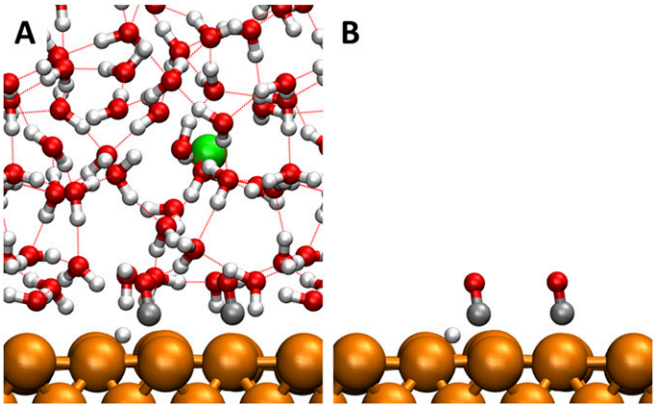

Fig. S1. Water/Cu(100) interface used in the calculations. *A* and *B* show the same system. *A* shows more details, including explicit water, Na^+, and hydrogen bond (HB) network. *B* removes water and Na^+ to show surface species (2 *CO and 1 H*). The colors are C in silver, H in white, O in red, Cu in orange, and Na in green. HBs are shown with red dashed line.

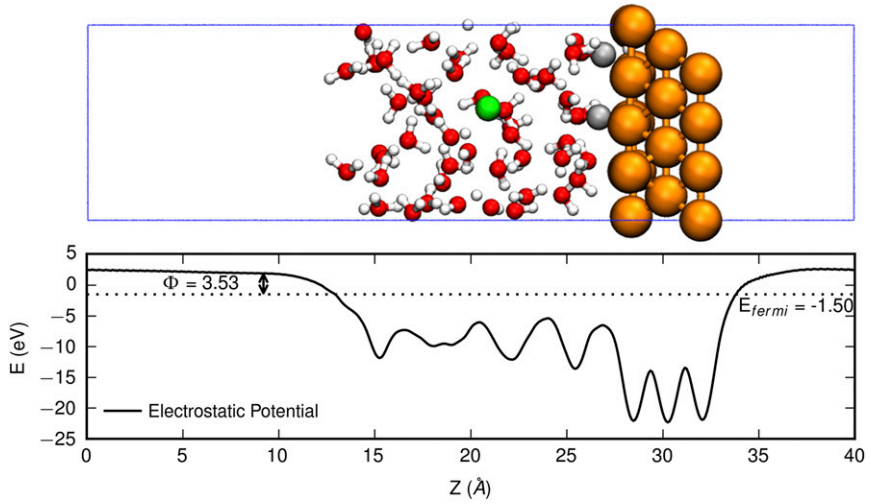

Fig. S2. Plane averaged electrostatic potential (in electronvolts) of water/Cu(100) electrode along the *z* direction. Indicated are the Fermi energy (E_{fermi}, in electronvolts) and the work function (Φ, in electronvolts). The atomic structure of the water/Cu(100) electrode is shown on the *Top* for viewing convenience. The colors are C in silver, H in white, O in red, Cu in orange, and Na in green. In this snapshot, $E_{fermi} = -1.50$ eV and $\Phi = 3.53$ eV.

Table S1. Collective variables (CVs) for various reduction steps of CH_4 formation on Cu(100) at pH 7 and 298 K

ID	Reaction equation	CV
1	$*CO + H* \rightarrow *CHO$	R(C–H)
1a	$*CO + H_2O + e^- \rightarrow *CHO + OH^-$	R(C–H)
1b	$*CO + H_2O + e^- \rightarrow *COH + OH^-$	R(O–H)
2	$*CHO + H_2O + e^- \rightarrow *CHOH + OH^-$	R(O–H)
2a	$*CHO + H* \rightarrow CH_2O$	R(C–H)
3	$*CHOH + e^- \xrightarrow{H_2O} *CH + OH^-$	R(C–O)
3a	$*CHOH + H* \rightarrow *CH_2OH$	R(C–H)
4	$*CH + H_2O + e^- \rightarrow *CH_2 + OH^-$	R(C–H)
4a	$*CH + H* \rightarrow *CH_2$	R(C–H)
5	$*CH_2 + H_2O + e^- \rightarrow *CH_3 + OH^-$	R(C–H)
5a	$*CH_2 + H* \rightarrow *CH_3$	R(C–H)
6	$*CH_3 + H_2O + e^- \rightarrow CH_4 + OH^-$	R(C–H)
6a	$*CH_3 + H* \rightarrow CH_4$	R(C–H)

Each number specifies the reduction step. Reaction IDs with only numbers are major reactions, whereas reaction IDs with a number plus a letter indicates a side reaction. H_2O on arrows are H_2O molecules involved in the Grotthuss hydrogen bond network to tunnel proton.

Table S2. Collective variables (CVs) for various reduction steps of C_2H_4 formation on Cu(100) at pH 7 and 298 K

ID	Reaction equation	CV
0	$*CO + *CO + \delta \cdot e^- \rightarrow *CO\text{–}CO^{\delta-}$	R(C–C)
1	$*OC\text{–}CO^{\delta-} + H_2O + (1-\delta) \cdot e^- \rightarrow *CO\text{–}COH + OH^-$	R(O–H)
2	$*CO\text{–}COH + H_2O + e^- \rightarrow *COH\text{–}COH + OH^-$	R(O–H)
2a	$*OC\text{–}CO^{\delta-} + H^* \rightarrow *CHO\text{–}CO^{\delta-}$	R(C–H)
3	$*COH\text{–}COH + e^- \xrightarrow{H_2O} *C\text{–}COH + OH^-$	R(C–H)
3a	$*COH\text{–}COH + H^* \rightarrow *CHOH\text{–}COH$	R(C–H)
4	$*C\text{–}COH + H_2O + e^- \rightarrow *CH\text{–}COH + OH^-$	R(C–H)
4a	$*C\text{–}COH + H^* \rightarrow *CH\text{–}COH$	R(C–H)
4b	$*C\text{–}COH + e^- \xrightarrow{H_2O} *C\text{–}C + OH^-$	R(C–O)
4c	$*C\text{–}COH + H^* \rightarrow *C\text{–}CHOH$	R(C–H)
5	$*CH\text{–}COH + e^- \xrightarrow{H_2O} *C\text{–}CH + OH^-$	R(C–O)
5a	$*CH\text{–}COH + H^* \rightarrow *CH_2\text{–}COH$	R(C–H)
5b	$*CH\text{–}COH + H^* \rightarrow *CH\text{–}CHOH$	R(C–H)
6	$*C\text{–}CH + H_2O + e^- \rightarrow *C\text{–}CH_2 + OH^-$	R(C–H)
6a	$*C\text{–}CH + H^* \rightarrow *C\text{–}CH_2$	R(C–H)
6b	$*C\text{–}CH + H_2O + e^- \rightarrow *CH\text{–}CH + OH^-$	R(C–H)
6c	$*C\text{–}CH + H^* \rightarrow *CH\text{–}CH$	R(C–H)
7	$*C\text{–}CH_2 + H_2O + e^- \rightarrow *CH\text{–}CH_2 + OH^-$	R(C–H)
7a	$*C\text{–}CH_2 + H^* \rightarrow *CH\text{–}CH_2$	R(C–H)
7b	$*C\text{–}CH_2 + H^* \rightarrow *C\text{–}CH_3$	R(C–H)
8	$*CH\text{–}CH_2 + H_2O + e^- \rightarrow C_2H_4 + OH^-$	R(C–H)
8a	$*CH\text{–}CH_2 + H^* \rightarrow C_2H_4$	R(C–H)
8b	$*CH\text{–}CH_2 + H_2O + e^- \rightarrow *CH\text{–}CH_3 + OH^-$	R(C–H)
8c	$*CH\text{–}CH_2 + H^* \rightarrow *CH\text{–}CH_3$	R(C–H)

Each number indicates the reduction step. Reaction IDs with only numbers are major reactions, and reaction IDs with a number plus a letter indicates a side reaction. H_2O on arrows are H_2O molecules involved in the Grotthuss hydrogen-bond network to tunnel proton.

Table S3. Free-energy barriers ($\Delta G^{\ddagger}$, in electronvolts) and free-energy differences (ΔG, in electronvolts) for various reduction steps of CH_4 formation on Cu(100) at pH 7 and 298 K

ID	Reaction equation	$\Delta G^{\ddagger}$, eV	ΔG, eV
1	$*CO + H^* \rightarrow *CHO$	0.96 (0.10)	0.90 (0.10)
1a	$*CO + H_2O + e^- \rightarrow *CHO + OH^-$	0.98 (0.07)	0.90 (0.08)
1b	$*CO + H_2O + e^- \rightarrow *COH + OH^-$	1.21 (0.13)	1.13 (0.11)
2	$*CHO + H_2O + e^- \rightarrow *CHOH + OH^-$	0.24 (0.15)	0.11 (0.12)
2a	$*CHO + H^* \rightarrow CH_2O$	1.01 (0.15)	0.51 (0.14)
3	$*CHOH + e^- \xrightarrow{H_2O} *CH + OH^-$	0.60 (0.06)	−0.04 (0.07)
3a	$*CHOH + H^* \rightarrow *CH_2OH$	0.86 (0.09)	0.38 (0.09)
4	$*CH + H_2O + e^- \rightarrow *CH_2 + OH^-$	0.41 (0.04)	0.32 (0.11)
4a	$*CH + H^* \rightarrow *CH_2$	0.97 (0.04)	0.19 (0.11)
5	$*CH_2 + H_2O + e^- \rightarrow *CH_3 + OH^-$	0.56 (0.10)	0.17 (0.13)
5a	$*CH_2 + H^* \rightarrow *CH_3$	1.05 (0.12)	0.01 (0.12)
6	$*CH_3 + H_2O + e^- \rightarrow CH_4 + OH^-$	0.82 (0.04)	−0.42 (0.11)
6a	$*CH_3 + H^* \rightarrow CH_4$	0.87 (0.14)	−0.69 (0.07)

The errors are in parentheses. All e^- are allowed to rearrange self-consistently during the AIMD simulations.

Table S4. Free-energy barriers ($\Delta G^{\ddagger}$, in electronvolts) and free-energy differences (ΔG, in electronvolts) for various reduction steps of C_2H_4 formation on Cu(100) at pH 7 and 298 K

ID	Reaction equation	$\Delta G^{\ddagger}$, eV	ΔG, eV
0	$*CO + *CO + \delta \cdot e^- \rightarrow *CO–CO^{\delta-}$	0.69 (0.11)	0.59 (0.13)
1	$*OC–CO^{\delta-} + H_2O + (1-\delta) \cdot e^- \rightarrow *CO–COH + OH^-$	0.14 (0.10)	−0.01 (0.07)
2	$*CO–COH + H_2O + e^- \rightarrow *COH–COH + OH^-$	0.02 (0.09)	−0.12 (0.11)
2a	$*OC–CO^{\delta-} + H^* \rightarrow *CHO–CO^{\delta-}$	1.12 (0.12)	0.56 (0.14)
3	$*COH–COH + e^- \xrightarrow{H_2O} *C–COH + OH^-$	0.63 (0.11)	0.43 (0.15)
3a	$*COH–COH + H^* \rightarrow *CHOH–COH$	1.07 (0.10)	0.80 (0.09)
4	$*C–COH + H_2O + e^- \rightarrow *CH–COH + OH^-$	0.45 (0.12)	0.22 (0.15)
4a	$*C–COH + H^* \rightarrow *CH–COH$	0.92 (0.10)	−0.01 (0.09)
4b	$*C–COH + e^- \xrightarrow{H_2O} *C–C + OH^-$	1.18 (0.10)	0.79 (0.10)
4c	$*C–COH + H^* \rightarrow *C–CHOH$	1.01 (0.09)	0.37 (0.11)
5	$*CH–COH + e^- \xrightarrow{H_2O} *C–CH + OH^-$	0.62 (0.11)	−0.11 (0.14)
5a	$*CH–COH + H^* \rightarrow *CH_2–COH$	1.41 (0.12)	1.22 (0.11)
5b	$*CH–COH + H^* \rightarrow *CH–CHOH$	1.05 (0.14)	0.83 (0.12)
6	$*C–CH + H_2O + e^- \rightarrow *C–CH_2 + OH^-$	0.61 (0.07)	0.20 (0.08)
6a	$*C–CH + H^* \rightarrow *C–CH_2$	0.93 (0.11)	0.40 (0.09)
6b	$*C–CH + H_2O + e^- \rightarrow *CH–CH + OH^-$	1.09 (0.08)	0.87 (0.09)
6c	$*C–CH + H^* \rightarrow *CH–CH$	1.41 (0.15)	0.68 (0.13)
7	$*C–CH_2 + H_2O + e^- \rightarrow *CH–CH_2 + OH^-$	0.50 (0.08)	0.38 (0.07)
7a	$*C–CH_2 + H^* \rightarrow *CH–CH_2$	1.10 (0.13)	0.42 (0.15)
7b	$*C–CH_2 + H^* \rightarrow *C–CH_3$	1.76 (0.09)	1.76 (0.09)
8	$*CH–CH_2 + H_2O + e^- \rightarrow C_2H_4 + OH^-$	0.39 (0.09)	−0.07 (0.10)
8a	$*CH–CH_2 + H^* \rightarrow C_2H_4$	1.15 (0.07)	0.02 (0.07)
8b	$*CH–CH_2 + H_2O + e^- \rightarrow *CH–CH_3 + OH^-$	0.70 (0.13)	0.70 (0.13)
8c	$*CH–CH_2 + H^* \rightarrow *CH–CH_3$	1.21 (0.12)	0.58 (0.11)

All e^- are allowed to rearrange self-consistently during the AIMD simulations.

Table S5. Work function (in electronvolts) of the initial state (Φ_0), transition state (Φ_{TS}), and final state (Φ_1) for various reduction steps of CH_4 formation on Cu(100) at pH 7 and 298 K

ID	Reaction equation	Φ_0, eV	Φ_{TS}, eV	Φ_1, eV
1	$*CO + H^* \rightarrow *CHO$	3.48 (0.33)	3.49 (0.23)	3.59 (0.24)
1a	$*CO + H_2O + e^- \rightarrow *CHO + OH^-$	3.48 (0.33)	3.60 (0.29)	3.80 (0.27)
1b	$*CO + H_2O + e^- \rightarrow *COH + OH^-$	3.48 (0.33)	3.52 (0.24)	3.75 (0.30)
2	$*CHO + H_2O + e^- \rightarrow *CHOH + OH^-$	3.38 (0.34)	3.48 (0.32)	3.66 (0.20)
2a	$*CHO + H^* \rightarrow CH_2O$	3.38 (0.34)	3.49 (0.32)	3.47 (0.27)
3	$*CHOH + e^- \xrightarrow{H_2O} *CH + OH^-$	3.36 (0.34)	3.55 (0.24)	3.80 (0.34)
3a	$*CHOH + H^* \rightarrow *CH_2OH$	3.36 (0.34)	3.47 (0.31)	3.49 (0.21)
4	$*CH + H_2O + e^- \rightarrow *CH_2 + OH^-$	3.23 (0.29)	3.42 (0.25)	3.70 (0.33)
4a	$*CH + H^* \rightarrow *CH_2$	3.23 (0.29)	3.28 (0.32)	3.39 (0.36)
5	$*CH_2 + H_2O + e^- \rightarrow *CH_3 + OH^-$	3.22 (0.29)	3.41 (0.23)	3.67 (0.29)
5a	$*CH_2 + H^* \rightarrow *CH_3$	3.22 (0.29)	3.25 (0.35)	3.32 (0.33)
6	$*CH_3 + H_2O + e^- \rightarrow CH_4 + OH^-$	3.26 (0.22)	3.42 (0.29)	3.63 (0.36)
6a	$*CH_3 + H^* \rightarrow CH_4$	3.26 (0.22)	3.38 (0.31)	3.40 (0.22)

Table S6. Work function (in electronvolts) of the initial state (Φ_0), transition state (Φ_{TS}), and final state (Φ_1) for various reduction steps of C_2H_4 formation on Cu(100) at pH 7 and 298 K

ID	Reaction equation	Φ_0, eV	Φ_{TS}, eV	Φ_1, eV
0	$*CO + *CO + \delta \cdot e^- \rightarrow *CO–CO^{\delta-}$	3.39 (0.24)	3.47 (0.28)	3.67 (0.3)
1	$*OC–CO^{\delta-} + H_2O + (1-\delta) \cdot e^- \rightarrow *CO–COH + OH^-$	3.67 (0.3)	3.75 (0.21)	3.74 (0.25)
2	$*CO–COH + H_2O + e^- \rightarrow *COH–COH + OH^-$	3.32 (0.30)	3.43 (0.35)	3.68 (0.29)
2a	$*OC–CO^{\delta-} + H^* \rightarrow *CHO–CO^{\delta-}$	3.67 (0.3)	3.76 (0.26)	3.83 (0.28)
3	$*COH–COH + e^- \xrightarrow{H_2O} *C–COH + OH^-$	3.13 (0.28)	3.27 (0.22)	3.50 (0.24)
3a	$*COH–COH + H^* \rightarrow *CHOH–COH$	3.13 (0.28)	3.28 (0.28)	3.19 (0.25)
4	$*C–COH + H_2O + e^- \rightarrow *CH–COH + OH^-$	3.43 (0.31)	3.61 (0.34)	3.80 (0.22)
4a	$*C–COH + H^* \rightarrow *CH–COH$	3.43 (0.31)	3.55 (0.35)	3.56 (0.35)
4b	$*C–COH + e^- \xrightarrow{H_2O} *C–C + OH^-$	3.43 (0.31)	3.48 (0.24)	3.72 (0.25)
4c	$*C–COH + H^* \rightarrow *C–CHOH$	3.43 (0.31)	3.56 (0.22)	3.60 (0.27)
5	$*CH–COH + e^- \xrightarrow{H_2O} *C–CH + OH^-$	3.28 (0.27)	3.42 (0.35)	3.65 (0.35)
5a	$*CH–COH + H^* \rightarrow *CH_2–COH$	3.28 (0.27)	3.36 (0.32)	3.40 (0.21)
5b	$*CH–COH + H^* \rightarrow *CH–CHOH$	3.28 (0.27)	3.29 (0.35)	3.38 (0.20)
6	$*C–CH + H_2O + e^- \rightarrow *C–CH_2 + OH^-$	3.43 (0.36)	3.60 (0.35)	3.85 (0.26)
6a	$*C–CH + H^* \rightarrow *C–CH_2$	3.43 (0.36)	3.46 (0.27)	3.57 (0.21)
6b	$*C–CH + H_2O + e^- \rightarrow *CH–CH + OH^-$	3.43 (0.36)	3.64 (0.25)	3.88 (0.29)
6c	$*C–CH + H^* \rightarrow *CH–CH$	3.43 (0.36)	3.48 (0.28)	3.60 (0.29)
7	$*C–CH_2 + H_2O + e^- \rightarrow *CH–CH_2 + OH^-$	3.26 (0.30)	3.45 (0.27)	3.64 (0.36)
7a	$*C–CH_2 + H^* \rightarrow *CH–CH_2$	3.26 (0.30)	3.32 (0.25)	3.44 (0.23)
7b	$*C–CH_2 + H^* \rightarrow *C–CH_3$	3.26 (0.30)	3.35 (0.29)	3.48 (0.26)
8	$*CH–CH_2 + H_2O + e^- \rightarrow C_2H_4 + OH^-$	3.24 (0.21)	3.38 (0.35)	3.65 (0.30)
8a	$*CH–CH_2 + H^* \rightarrow C_2H_4$	3.24 (0.21)	3.30 (0.29)	3.43 (0.24)
8b	$*CH–CH_2 + H_2O + e^- \rightarrow *CH–CH_3 + OH^-$	3.24 (0.21)	3.44 (0.20)	3.67 (0.32)
8c	$*CH–CH_2 + H^* \rightarrow *CH–CH_3$	3.24 (0.21)	3.34 (0.26)	3.44 (0.28)

Table S7. Corrected free-energy barriers ($\Delta G^{\ddagger}$, in electronvolts) and corrected free-energy differences (ΔG, in electronvolts) for various reduction steps of CH_4 formation on Cu(100) at pH 7 and 298 K

ID	Reaction equation	$\Delta G^{\ddagger}$, eV	ΔG, eV
1	$*CO + H^* \rightarrow *CHO$	0.96	0.89
1a	$*CO + H_2O + e^- \rightarrow *CHO + OH^-$	0.97	0.82
1b	$*CO + H_2O + e^- \rightarrow *COH + OH^-$	1.21	1.07
2	$*CHO + H_2O + e^- \rightarrow *CHOH + OH^-$	0.24	0.05
2a	$*CHO + H^* \rightarrow CH_2O$	1.01	0.50
3	$*CHOH + e^- \xrightarrow{H_2O} *CH + OH^-$	0.59	−0.19
3a	$*CHOH + H^* \rightarrow *CH_2OH$	0.86	0.37
4	$*CH + H_2O + e^- \rightarrow *CH_2 + OH^-$	0.40	0.15
4a	$*CH + H^* \rightarrow *CH_2$	0.97	0.17
5	$*CH_2 + H_2O + e^- \rightarrow *CH_3 + OH^-$	0.55	0.01
5a	$*CH_2 + H^* \rightarrow *CH_3$	1.05	0.00
6	$*CH_3 + H_2O + e^- \rightarrow CH_4 + OH^-$	0.81	−0.53
6a	$*CH_3 + H^* \rightarrow CH_4$	0.86	−0.71

The work functions are referenced to the initial states.

Table S8. Corrected free-energy barriers ($\Delta G^{\ddagger}$, in electronvolts) and corrected free-energy differences (ΔG, in electronvolts) for various reduction steps of C_2H_4 formation on Cu(100) at pH 7 and 298 K

ID	Reaction equation	$\Delta G^{\ddagger}$, eV	ΔG, eV
0	$*CO + *CO + \delta \cdot e^- \rightarrow *CO\text{–}CO^{\delta-}$	0.69	0.56
1	$*OC\text{–}CO^{\delta-} + H_2O + (1-\delta) \cdot e^- \rightarrow *CO\text{–}COH + OH^-$	0.14	−0.01
2	$*CO\text{–}COH + H_2O + e^- \rightarrow *COH\text{–}COH + OH^-$	0.02	−0.17
2a	$*OC\text{–}CO^{\delta-} + H^* \rightarrow *CHO\text{–}CO^{\delta-}$	1.12	0.55
3	$*COH\text{–}COH + e^- \xrightarrow{H_2O} *C\text{–}COH + OH^-$	0.62	0.38
3a	$*COH\text{–}COH + H^* \rightarrow *CHOH\text{–}COH$	1.06	0.80
4	$*C\text{–}COH + H_2O + e^- \rightarrow *CH\text{–}COH + OH^-$	0.44	0.17
4a	$*C\text{–}COH + H^* \rightarrow *CH\text{–}COH$	0.91	−0.02
4b	$*C\text{–}COH + e^- \rightarrow *C\text{–}C + OH^-$	1.18	0.76
4c	$*C\text{–}COH + H^* \rightarrow *C\text{–}CHOH$	1.00	0.36
5	$*CH\text{–}COH + e^- \xrightarrow{H_2O} *C\text{–}CH + OH^-$	0.61	−0.16
5a	$*CH\text{–}COH + H^* \rightarrow *CH_2\text{–}COH$	1.41	1.21
5b	$*CH\text{–}COH + H^* \rightarrow *CH\text{–}CHOH$	1.05	0.83
6	$*C\text{–}CH + H_2O + e^- \rightarrow *C\text{–}CH_2 + OH^-$	0.60	0.13
6a	$*C\text{–}CH + H^* \rightarrow *C\text{–}CH_2$	0.93	0.39
6b	$*C\text{–}CH + H_2O + e^- \rightarrow *CH\text{–}CH + OH^-$	1.07	0.79
6c	$*C\text{–}CH + H^* \rightarrow *CH\text{–}CH$	1.41	0.67
7	$*C\text{–}CH_2 + H_2O + e^- \rightarrow *CH\text{–}CH_2 + OH^-$	0.49	0.32
7a	$*C\text{–}CH_2 + H^* \rightarrow *CH\text{–}CH_2$	1.10	0.41
7b	$*C\text{–}CH_2 + H^* \rightarrow *C\text{–}CH_3$	1.76	1.74
8	$*CH\text{–}CH_2 + H_2O + e^- \rightarrow C_2H_4 + OH^-$	0.38	−0.14
8a	$*CH\text{–}CH_2 + H^* \rightarrow C_2H_4$	1.15	0.01
8b	$*CH\text{–}CH_2 + H_2O + e^- \rightarrow *CH\text{–}CH_3 + OH^-$	0.68	0.63
8c	$*CH\text{–}CH_2 + H^* \rightarrow *CH\text{–}CH_3$	1.21	0.56

The work functions are referenced to the initial states.